Received January 10, 2020, accepted February 7, 2020, date of publication February 20, 2020, date of current version March 9, 2020.

Digital Object Identifier 10.1109/ACCESS.2020.2974491

High-Performance Nano-Sensing and Slow-Light Applications Based on Tunable Multiple Fano Resonances and EIT-Like Effects in Coupled Plasmonic Resonator System

SHUO WANG, TONGGANG ZHAO, SHILIN YU, AND WENYUAN MA
School of Electronic Engineering, Beijing University of Posts and Telecommunications, Beijing 100876, China

Corresponding authors: Shuo Wang (wangshuo_bupt@bupt.edu.cn) and Tonggang Zhao (zhaotg@bupt.edu.cn)

This work was supported by the National Natural Science Foundation of China under Grant 61835002 and Grant 61631014.

ABSTRACT A basic plasmonic system, consisting of a stub metal-insulator-metal (MIM) waveguide coupled with a ring resonator, is presented to realize Fano resonance and electromagnetically induced transparency-like (EIT-like) effect, which are numerically calculated by the finite element method (FEM). Meanwhile, the formation mechanism of Fano resonance is analyzed according to numerical simulations. Besides, the coupled mode theory (CMT) and the standing wave theory are used for explaining the Fano and EIT-like resonances phenomenon. Based on this system, an inner ring cavity is connected to the ring resonator by a slot and another ring cavity is later introduced under the stub resonator in order to constitute a new coupled plasmonic resonator system, providing quadruple Fano resonances and double EIT-like responses finally. In addition, the Fano and EIT-like resonances can be independently tuned by adjusting the structural parameters, which makes the design of highly integrated photonic circuits more flexible. The main contribution of this paper is that the proposed structure has a relatively good sensitivity of 1600 nm/RIU and an ultra-high FOM value of 1.2×10^6 as a refractive index nanosensor. Moreover, it can serve as an all-optical switch with a high on/off extinction ratio of about 43 dB. Additionally, its maximum group delay time and group index are about 1.49 ps and 221, indicating that the proposed system has a pretty good slow light effect. Therefore, the proposed structures are believed to have significant applications in high-performance nanosensors, switches, slow light devices and nonlinear areas in highly integrated plasmonic devices.

INDEX TERMS Multiple EIT-like effects, multiple Fano resonances, refractive index sensor, surface plasmon polaritons (SPPs), slow light, ultra-high FOM.

I. INTRODUCTION

With the development of optical technology, future integrated optics will have higher requirements on the density of integration. Surface plasmon polaritons (SPPs), which can control the propagation of optical signal in nanoscale because of their strong field confinement to the interface of the metal and dielectric [1], [2], show a great prospect in the application of subwavelength optical devices and highly integrated photonic circuits [3].

So far, there have been numerous SPPs guiding structures like metal nanoparticle waveguides, metal films [4], metal-insulator-metal (MIM) slabs [5]–[8], plasmonic nanoclusters [9], [10], nano-slits [11], and hybrid Bragg waveguides, among which the MIM waveguide has the advantages of deep-subwavelength confinement [12], low bend losses [18] and easy integration [13], [14]. Therefore, it has crucial applications in highly integrated optical devices [15]–[17]. Based on the MIM waveguide, enormous devices, like plasmonic nanosensors [18]–[21], slow light devices [22]–[24], all-optical switches [25], filters [26], splitters [27], and demultiplexers [28] have been investigated in theory and simulation. Among them, plasmonic nano-sensing was rated as one of the top ten emerging technologies by Scientific American in 2018 [29]. Therefore, a growing number of researches are focusing on designing high-performance nano-sensors in MIM waveguide coupled resonators. Some novel physical features like Fano resonance

The associate editor coordinating the review of this manuscript and approving it for publication was Chao Zuo.

and electromagnetically induced transparency (EIT)-like effect [30], [31] have important applications in refractive index sensors, because a tremendous linear shift of EIT-like and Fano resonance can be caused by a minimal environmental change [31]. Fano resonance is the coupling effect arising from the interaction between narrow discrete states (dark modes) and broad continuous state (bright mode) [32]–[34]. The Fano resonance can also be originally deemed as the classical analogue of EIT under certain conditions [35]. In comparison with Fano resonance, EIT is a quantum interference phenomenon with a narrow optical enhanced transmission spectrum as a result of the quantum destructive interference between the atomic resonances [36]. Previous researches indicate that an optical phenomenon similar to EIT, which is termed as EIT-like effect, can occur in the coupled plasmonic resonator system [37]. As a quantum interference effect [38], [39], EIT is exceedingly sensitive to alteration in the refractive index. Consequently, the EIT-like and Fano resonances show great potential in high-performance plasmonic sensors [40]. When it comes to the sensor, its sensitivity and figure of merit (FOM) are vital for evaluating the sensing performance of the system. Compared with single Fano or EIT-like resonance system, the multiple Fano and EIT-like resonances have attracted enormous attention [41]–[43], because they may provide more reliable results and even realize multi-spectrum sensor and they will have more dominance in highly integrated photonic circuits due to their parallel processing capability. However, because a majority of proposed multiple Fano or EIT-like resonances arise from multimode coupling between the resonators [17], [18], it is hard to extend them to more Fano and EIT-like resonances and make an independent and precise tailoring.

In this research, tunable multiple Fano and EIT-like resonances with a great sensitivity and a large FOM value are achieved in coupled plasmonic resonator system. First of all, a plasmonic system consisting of a stub MIM waveguide and a ring resonator is designed as a basic structure. The transmission spectrum, the phase shift and magnetic field H_z distributions are numerically calculated in COMSOL Multiphysics by the finite element method (FEM). Meanwhile, the formation mechanism of Fano resonance is analyzed based on the transmission spectra and magnetic field distribution. Moreover, the transmission property can be well fitted by the coupled mode theory (CMT). According to the standing wave theory, Fabry-Perot (FP) cavity theory and TM mode theory, the resonant order N is calculated by formulas and corresponds well with the numerical results in simulations. Based on the basic structure, an inner ring cavity is connected to the ring resonator by a slot, and a ring cavity is later placed under the stub resonator to create a new coupled plasmonic structure, providing quadruple Fano resonances and double EIT-like effects, finally. Additionally, these multiple Fano and EIT-like resonances can be independently controlled by adjusting the dimensions of the slot or inner ring cavity since they stem from different mechanisms. Simulation results also indicate that the new system can act as an excellent nanosensor with a great sensitivity of 1600 nm/RIU and an ultra-high FOM of 1.2×10^6 and an optical switch with a high extinction ratio of about 43 dB which is higher than that of the optical switch in the references [7], [59], [60]. In comparison with the recent works [6], [7], [18]–[21], [40]–[45], [53], [55], our nanosensor performs better than most of them. Besides, a maximum group delay time and group index about 1.49 ps and 221 can be realized, which outperform the slow light devices in the references [20], [54]–[57]. Based on the ultra-high FOM, independent tunability and favorable expansibility of the multiple Fano and EIT-like effects, the proposed structure with its outstanding performance can be applied to highly integrated photonic devices, such as bio-chemical sensors, slow light devices, optical switches and filters.

II. STRUCTURE MODEL AND THEORETICAL ANALYSIS

The basic proposed structure is displayed in figure 1, and consists of a stub MIM waveguide coupled to a ring resonator. The gray part of the two-dimensional diagram represents silver, and the white etches in between are filled with air. The total length of the proposed structure is D, and the height of the stub is H. The center of the ring is O_1. The dimensions are fixed as: $D = 2$ um, $H = 150$ nm, $R = 250$ nm, $\overline{R} = 225$ nm, which further simplifies the calculation. Due to the restriction of the nanofabrication techniques the coupling distance between the stub resonator and the composite structure g is chosen to be 10 nm. The widths of the MIM waveguide and the stubs, and the thickness of the ring cavity are all set to $w = 50$ nm so as to allow only the fundamental mode (TM_0) to propagate in the structure.

To explore the optical properties of the basic system, its transmission spectra are numerically calculated by FEM, which is displayed in figure 2. And it reveals that the system exhibits the Fano resonance and EIT-like response at 680 and 989 nm, called FR and EIT. Additionally, the transmittance of SPPs is expressed as $T = P_{\text{with}}/P_{\text{without}}$, here P_{with} and P_{without} stand for the SPPs power flows of the port with and without ring cavity, respectively [44]. And the dispersion relation of the TM mode is given as [47]:

$$\varepsilon_m k_d \tanh\left(\frac{wk_d}{2}\right) + \varepsilon_d k_m = 0 \tag{1}$$

And k_d and k_m are

$$k_d = \sqrt{\beta^2 - \varepsilon_d k_0^2}, \quad k_m = \sqrt{\beta^2 - \varepsilon_m k_0^2} \tag{2}$$

$$n_{eff} = \beta/k_0 \tag{3}$$

where k_d and k_m are transverse propagation constants in air and silver, separately. k_0 is the free space wave vector. β is the propagation constant of the SPPs wave. n_{eff} is the effective refractive index of the SPPs in the MIM waveguide. ε_d and ε_m are the dielectric constants of the dielectric air ($\varepsilon_d = 1.0$) and the metal silver, separately. To describe the silver analytically, Drude model [46] is adopted and later implemented in the

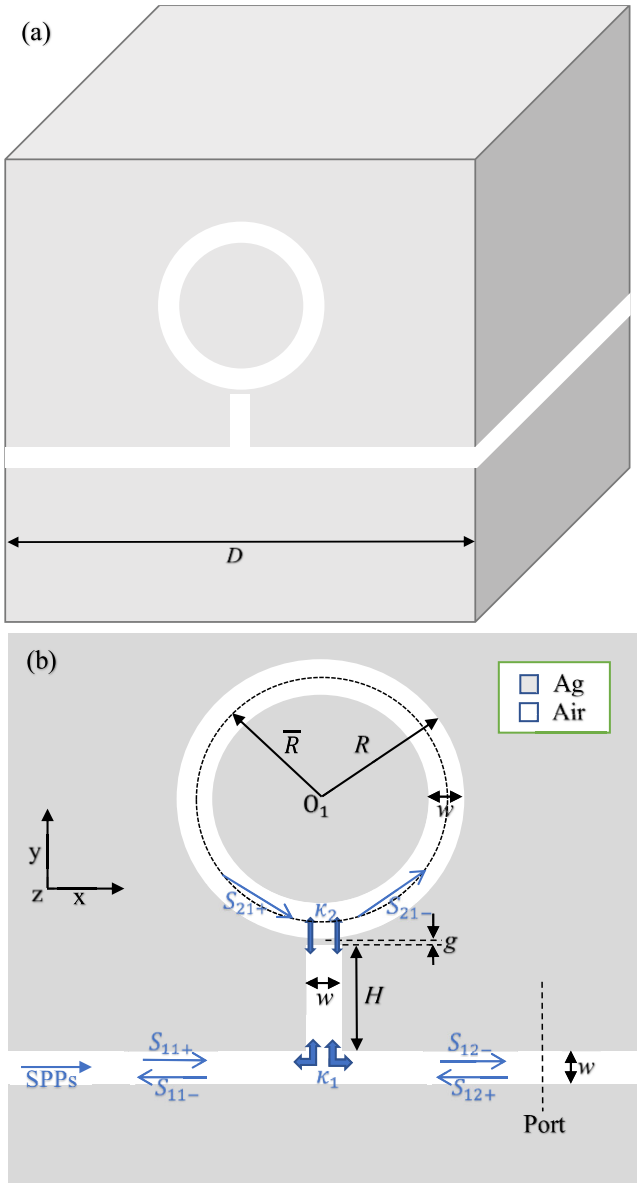

FIGURE 1. (a) Schematic diagram of the basic proposed structure. (b) Cross-section profile of the basic proposed structure.

software by interpolation. The model gives the permittivity of the silver in relation to the frequency as such:

$$\varepsilon_m(\omega) = \varepsilon_\infty - \frac{\omega_p^2}{\omega^2 + i\omega\gamma}, \tag{4}$$

where $\varepsilon_\infty = 3.7$, $\omega_p = 9.1\text{eV}$, and $\gamma = 0.018\text{eV}$.

The resonance wavelength of MIM waveguide coupled resonator can be derived on the basis of the standing wave theory [28], [48] as

$$\lambda = \frac{2n_{eff}L}{N - \phi/\pi}, \quad N = 1, 2, 3\ldots \tag{5}$$

Here L is the length of the resonator, N is the resonant order,ϕ is the phase shift brought about by the SPPs reflection off the metal wall in the resonator. Based on equations (2)-(3),

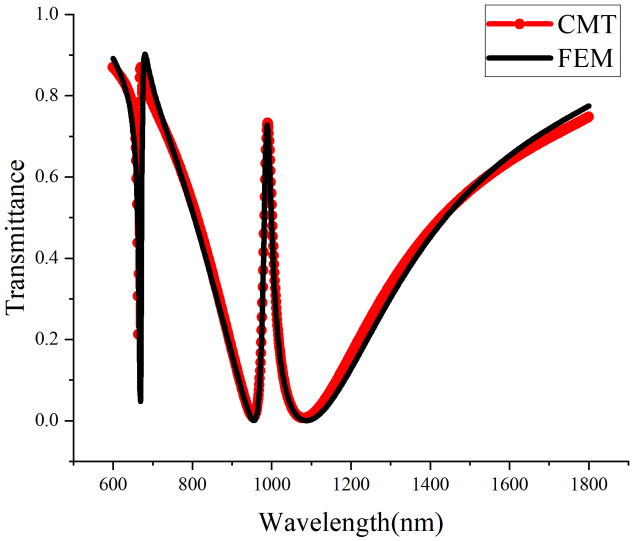

FIGURE 2. Transmission spectra of the basic structure calculated by FEM (black solid line) and CMT (red dot line).

the n_{eff} can be derived as

$$n_{eff} = \sqrt{[\varepsilon_m + \left(\frac{k_m}{k_0}\right)^2]} \tag{6}$$

In order to analyze the Fano resonance and EIT-like effect, the CMT is used for explaining the transmission property. The amplitudes of the input and output SPPs waves of the resonator are denoted by S_{11+}, S_{11-}, S_{12+}, S_{12-}, S_{21+}, and S_{21-}, which are depicted in figure 1(b). When the SPPs wave with a frequency ω is launched into the system from the input port of the MIM waveguide ($S_{12+} = 0$), the time evolution of the field amplitude A_1 of the stub resonator can be expressed as [52], [53]:

$$\frac{dA_1}{dt} = \left(-j\omega_1 - \frac{1}{\tau_0} - \frac{1}{\tau_1} - \frac{1}{\tau_2}\right)A_1 + \kappa_1 e^{j\theta_1} S_{11+} + \kappa_2 e^{j\theta_2} S_{21+} \tag{7}$$

$$S_{21+} = \delta e^{j\varphi} S_{21-} \tag{8}$$

$$S_{12-} = S_{11+} - \kappa_1 e^{-j\theta_1} A_1, \quad \kappa_1 = \sqrt{\frac{1}{\tau_1}} \tag{9}$$

$$S_{21-} = -S_{21+} + \kappa_2 e^{-j\theta_2} A_1, \quad \kappa_2 = \sqrt{\frac{2}{\tau_2}}. \tag{10}$$

Here, ω_1 is the resonance frequency of the stub resonator. j is the imaginary unit ($j^2 = -1$). The decay time of internal loss in the stub resonator is τ_0. τ_1 and τ_2 are the decay time from the stub to coupling waveguide and coupling cavity. κ_1 is the coupling coefficient between the stub resonator and MIM waveguide, and κ_2 is the coupling coefficient between the stub resonator and the composite cavity. θ_i ($i = 1, 2$) is the phase of the coupling coefficient. φ and δ are the phase change and amplitude attenuation between input and output SPPs waves of the stub resonator.

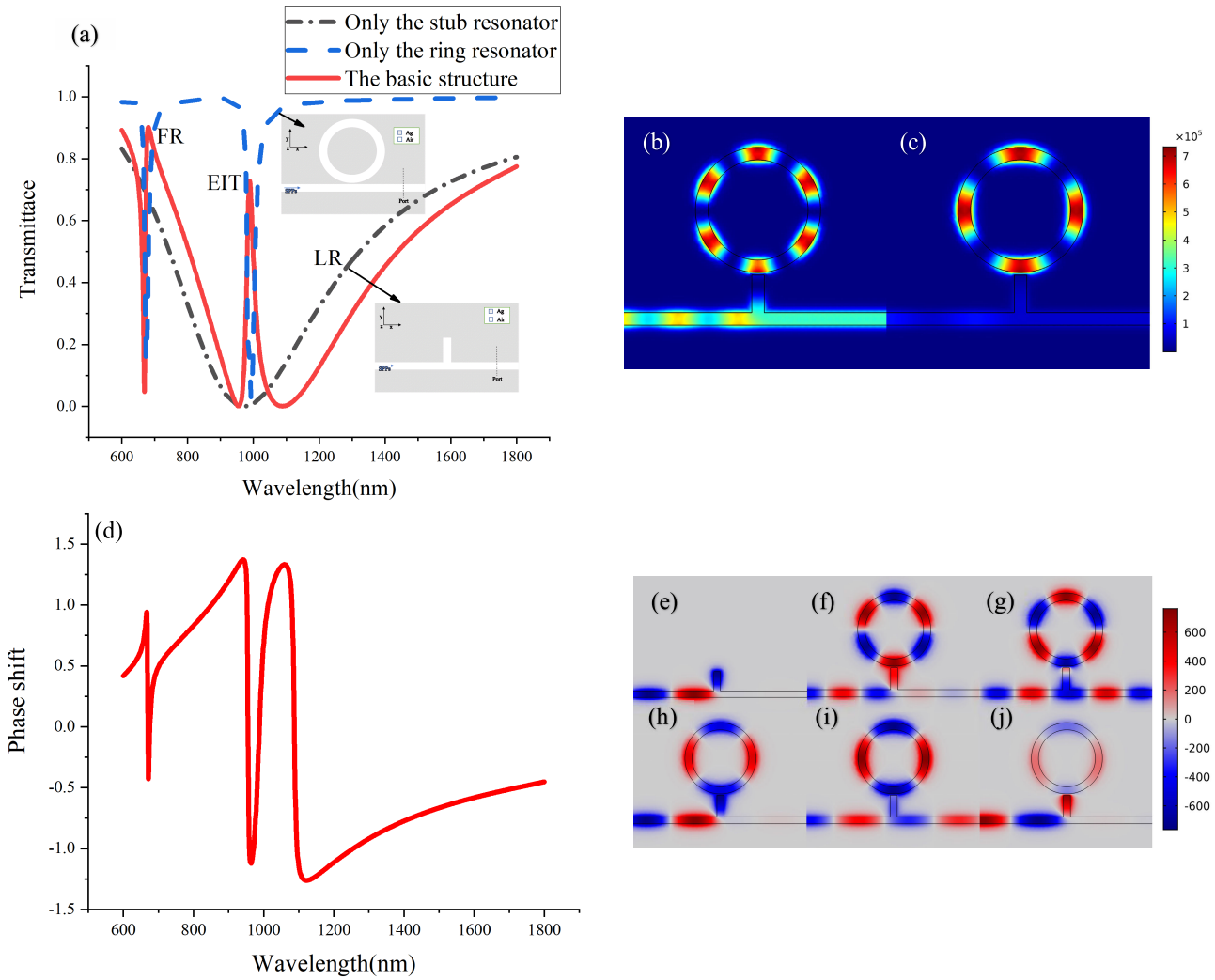

FIGURE 3. (a) The black, blue and red lines denote the transmission spectrum of the stub MIM waveguide, the MIM waveguide with the ring cavity and the basic structure, respectively. (b)-(c) The distribution of magnetic field intensity ($|H_z|^2$) at $\lambda = 680$ nm (FR peak) and 989 nm (EIT peak). (d) The phase shift spectrum of the basic proposed structure. (e) The H_z field distribution at $\lambda = 971$ nm without ring cavity. (f)-(j) The H_z field distribution at $\lambda = 669$ nm (FR valley), $\lambda = 680$ nm (FR peak), $\lambda = 955$ nm (EIT valley),$\lambda = 989$ nm (EIT peak) and $\lambda = 1088$ nm (EIT valley).

According to equations (7)-(10), the transmission T of the proposed system above can be worked out and expressed as:

$$T(\omega) = \left|\frac{S_{12-}}{S_{11+}}\right|^2 = \left|\frac{j(\omega_1-\omega)+\frac{1}{\tau_0}+\frac{1}{\tau_2}(1-\delta e^{j\varphi})/(1+\delta e^{j\varphi})}{j(\omega_1-\omega)+\frac{1}{\tau_0}+\frac{1}{\tau_1}+\frac{1}{\tau_2}(1-\delta e^{j\varphi})/(1+\delta e^{j\varphi})}\right|^2 \quad (11)$$

Here, the phase term φ can be described as [61]:

$$\varphi(\omega) = \frac{\omega n_{eff} L}{c} + \theta \quad (12)$$

where, θ is the additional phase shift of the stub waveguide. c is the speed of light in vacuum. In order to prove the accuracy of the research results in theory, we use the equation (11) to fit the simulation results based on CMT theory. The red dotted line in figure 2 is the fitting result, and the parameters of equation (11) are set as $\omega_1 = 1.8095 \times 10^{15}$ rad/s, $\tau_0 = 64.3824$ fs, $\tau_1 = 2.1310$ fs, $\tau_2 = 12.8279$ fs, $\delta = 0.9718$, $\theta = 0.05\pi$. Obviously, the fitting result is in good agreement with the simulation result.

To study the formation mechanism of Fano resonance, figure 3(a) shows the transmission spectra of the MIM waveguide with the stub resonator and with the ring cavity and the basic system. From this figure, it is found that the stub MIM waveguide shows a broadband transmission spectrum (the black dash dot line) called Lorentzian-like resonance marked as LR, whereas the ring cavity exhibits a narrow discrete spectrum (the blue dash line). Evidently, two sharp asymmetric transmission peaks are generated respectively near the corresponding positions of the two transmission valleys on the blue curve in figure 3 (a). Therefore, the formation of the FR and EIT can be explained by the interaction of the narrow discrete resonances (dark modes) of the ring cavity and the broad continuum resonance (bright mode) of the stub resonator. The asymmetric profiles FR and EIT originate from the reverse coherence properties

(destructive or constructive) near the opposite sides of the resonant wavelength [18], [41], [42].

In order to further comprehend the underlying physics of these Fano resonances in the proposed system, the corresponding field intensity ($|H_z|^2$) distributions at $\lambda = 680$ nm (FR peak) and 989 nm (EIT peak) are shown in figure 3 (b)-(c). Obviously, nearly all the energy is trapped in the ring resonator, separately exciting the standing wave pattern with $N = 6$ and $N = 4$. These high-order resonant modes are the dark modes with a narrowband response spectrum supported by the ring cavity. However, the bright mode with a broadband transmission spectrum is supported by the stub resonator. Therefore, the dark modes interfere with the bright mode, generating the FR and EIT line-shape. Based on equations (4)-(6), the incident wavelength $\lambda = 680$ nm (FR peak) / 989 nm (EIT peak) corresponds to the effective SPPs wavelength of $\lambda_{spp} = \frac{\lambda}{n_{eff}} = 485$ nm / 716 nm, so $N = \frac{2n_{eff}L}{\lambda} = \frac{2L}{\lambda_{spp}} = 2(2\pi\overline{R})/\lambda_{spp} = 5.83 \approx 6/3.95 \approx 4$, which is consistent with the result of the numerical calculation in figure 3 (b)-(c). Thus, we can make a simple inference that both FR and EIT are mainly affected by the $N = 6$ order ring mode and $N = 4$ order ring mode, respectively. Besides, the simulated phase shift of the system is drawn in figure 3(d). Compared with figure 3(a), the wavelengths of rapid phase shift change in figure 3(d) coincide well with the resonant wavelengths of FR and EIT, respectively.

To further investigate the underlying principle of these Fano resonances, the Hz field distributions at the incident wavelength $\lambda = 669$ nm (FR valley), $\lambda = 680$ nm (FR peak), $\lambda = 955$ nm (EIT valley), $\lambda = 971$ nm (LR valley), $\lambda = 989$ nm (EIT peak) and $\lambda = 1088$ nm (EIT valley). As illustrated in figure 3(e), without ring cavity, there is anti-phase between the stub resonator and MIM waveguide at the wavelength of 971 nm. And the SPPs are coupled to the stub cavity. Then, they are completely reflected from the top of the stub cavity to form a strong standing wave pattern, which inhibits SPPs from continuing to transmit to the output of the waveguide and forms a transmission valley. By observing figure 3(f), it is obvious that the H_z fields are anti-phase between the stub resonator and MIM waveguide, which induces destructive interference between the incident light and the light escaping into the MIM waveguide from the stub resonator and transmission suppression. Nevertheless, the H_z fields shown in figure 3(g) indicate that an in-phase relationship is noticeable between the stub resonator and MIM waveguide, which causes constructive interference between the two excitation pathways and transmission enhancement. Therefore, the power flow is confined to the stub and ring cavity, and the dark mode from the ring cavity interferes with the bright mode from stub resonator, resulting in FR. From the H_z field distributions at $\lambda = 955$ nm and $\lambda = 1088$ nm which are shown in figure 3 (h) and (j), it can be observed that there are anti-phase between the stub resonator and input MIM waveguide, namely the condition of resonance destructive is met, giving rise to the destructive interference between the two optical paths and transmission suppression. Whereas for $\lambda = 989$ nm (the EIT peak), which is shown in figure 3(i), the H_z fields in the poorly coupled stub resonator are in-phase with the H_z fields in input MIM waveguide, which causes the coherence enhancement to generate the EIT-like phenomenon [47], [51]. Therefore, the dark mode supported by the ring cavity interferes with the bright mode from stub resonator, leading to EIT. As shown in figure 3(j), a strong magnetic field emerges in the stub resonator, whereas extremely week magnetic field appears in the ring resonator. It indicates that the SPPs do not resonate in the ring cavity because the incident wavelength ($\lambda = 1088$ nm) is far from the resonant wavelength ($\lambda = 955$ nm) of the ring cavity.

III. MULTIPLE FANO AND EIT-LIKE RESONANCES INDUCED BY CONNECTING AN INNER RING CAVITY TO THE RING RESONATOR THROUGH A SLOT

The basic proposed structure above is well malleable and can be easily extended to a quadruple Fano resonances and double EIT-like responses system by connecting an inner ring cavity to the ring resonator through a slot and adding a ring cavity under the stub.

IV. TRIPLE FANO RESONANCES INDUCED BY CONNECTING AN INNER RING CAVITY TO THE RING RESONATOR THROUGH A SLOT

To further research the basic structure discussed above, an inner ring cavity is connected to the ring resonator by a slot, which is plotted in figure 4(a). Herein, the length of the slot is $k = 60$ nm, and the center of the inner disk is O_2. The radius of the inner ring is $R_0 = 130$ nm, and the width of the inner ring is fixed as $w = 50$ nm. Besides, other parameters are the same as the structure in section II. In figure 4(b), comparing with the transmission spectrum of the basic structure, it can be observed that the resonant wavelengths of FR and EIT are slightly moved, and two new Fano resonance line-shapes arise due to the structural breaking [33], [34], [62], marked as NFR1 and NFR2. This is because the symmetry of the basic structure is broken after the introduction of the end-coupled cavity. According to the reference [62], new higher-order resonant modes (dark modes) will be generated, which interfere with the bright mode generated by the stub cavity to produce new Fano resonances. At the same time, based on equation (5), the resonant wavelength is proportional to the length of the resonator, and inversely proportional to the order of the resonant mode. Nevertheless, the change caused by the increase of the length of the resonant and the increase of the resonant order which is caused by the structural breaking do not cancel each other out, so the resonant wavelengths of FR and EIT are slightly moved. Next, we can still change the resonant wavelength of the derived structure by adjusting the length of the cavity. To investigate the formation mechanisms of the Fano resonances in the derived structure, the phase shift spectrum of the derivative structure and the field intensity ($|H_z|^2$) distributions at $\lambda = 650$ nm (FR peak), 795 nm (NFR1 peak), 973 nm (EIT peak), and 1560 nm

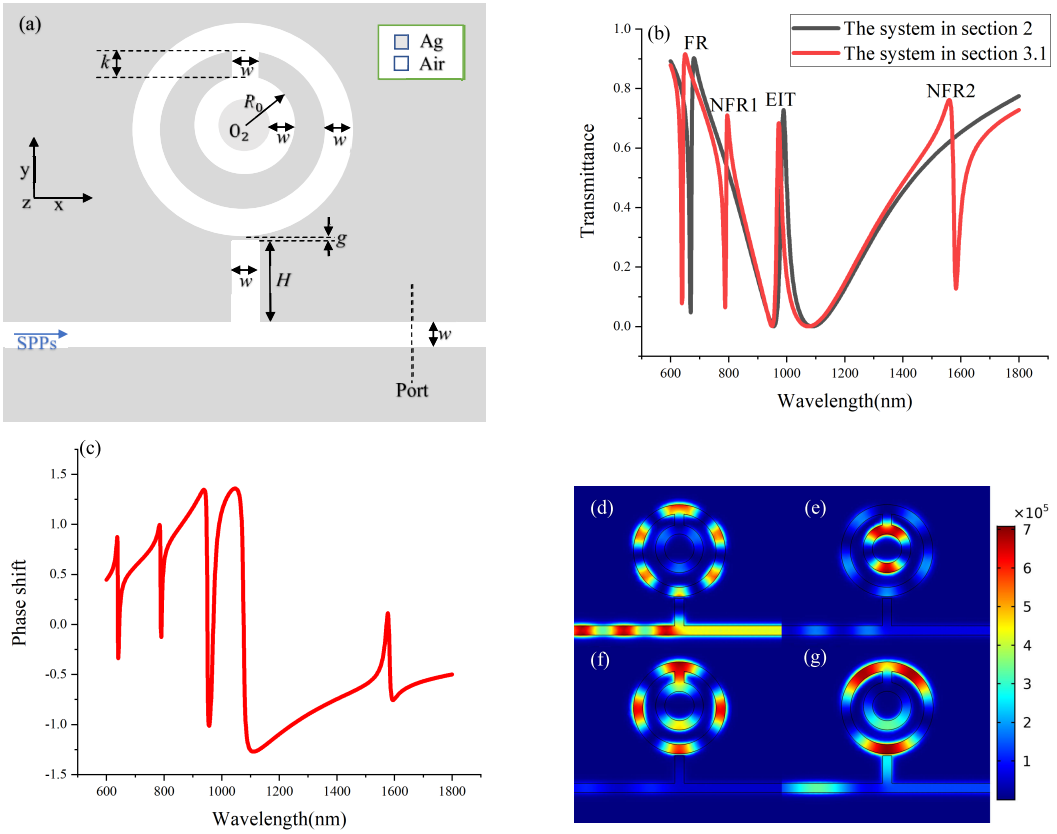

FIGURE 4. (a) Schematic diagram of the derived structure in section III.A (b) The black and red lines stand for the transmission spectrum of the basic proposed structure and the derived structure. (c) The phase shift spectrum of the derived structure. (d)-(g) The distribution of magnetic field intensity ($|H_z|^2$) at $\lambda = 650$ nm (FR peak), 795 nm (NFR1 peak), 973 nm (EIT peak), and 1560 nm (NFR2 peak).

(NFR2 peak) are displayed in figure 4(c)-(g), respectively. In comparison with figure 4(b), the wavelengths of rapid phase shift change in figure 4(c) are coincident with the resonant wavelengths of FR, NFR1, EIT and NFR2, respectively. As shown in figure 4(d), almost all the energy is limited in the ring resonator to excite a narrow high-order resonant mode (dark mode). And the dark mode interferes with the broad low-order resonant mode (bright mode) resulting from stub resonator to produce FR, which indicates that FR is mainly influenced by the ring mode, namely the resonant wavelengths of FR is redshifted with the length of the ring cavity increasing. Similarly, it is noticed that almost all the energy is confined in the inner ring cavity, which indicates that the inner ring cavity is coupled to the ring cavity and produces a new narrow high-order mode termed as inner ring mode from figure 4(e). Namely, NFR1 is mainly produced by inner ring mode. Whereas EIT and NFR2 are mainly affected by the ring-inner ring mode according to figure 4 (f) and (g). In this system, the inner ring mode and the ring-inner ring mode are dark modes, and they are coupled with the bright mode form stub to result in NFR1, EIT and NFR2. Therefore, we can tune these Fano resonances by changing the structural parameters.

To further test the analysis above, the transmission spectra of the derived structure are studied by altering the structural parameters. According to equation (5), the resonant wavelength has linear redshift as the length of the resonator increases. When the length of the slot k increases from 20 nm to 80 nm with a step of 20 nm with other parameters kept constant, the resonant wavelengths are nearly linear redshifted, which is displayed in figure 5(a). To further verify this linear dependence, the resonant wavelengths of FR, NFR1, EIT and NFR2 are calculated, and the results do exhibit this linear characteristic, which are illustrated in figure 5(b). In addition, the influence of R_0, which alters from 110 nm to 140 nm with a step of 10 nm, on the transmission spectra is investigated, and the results are shown in figure 5(c). It is obvious that FR resonance peak is slightly moved, affirming that FR is mainly induced by the ring mode, and it is also affected by the inner ring mode to a small degree. Thus they will be slightly influenced by variable R_0, which is identical to the results of previous analysis. And the resonant wavelengths of EIT and NFR2 have an evident redshift on account of the fact that EIT and NFR2 are mainly influenced by the ring-inner ring mode. Evidently, the NFR1 have a more drastic redshift because it primarily originates from the inner ring mode. In a similar way, the resonant wavelengths of FR, NFR1, EIT and NFR2 are calculated, which are shown in figure 5(d). Through the adjustment of the structural parameters, the derived system can be better tuned and controlled.

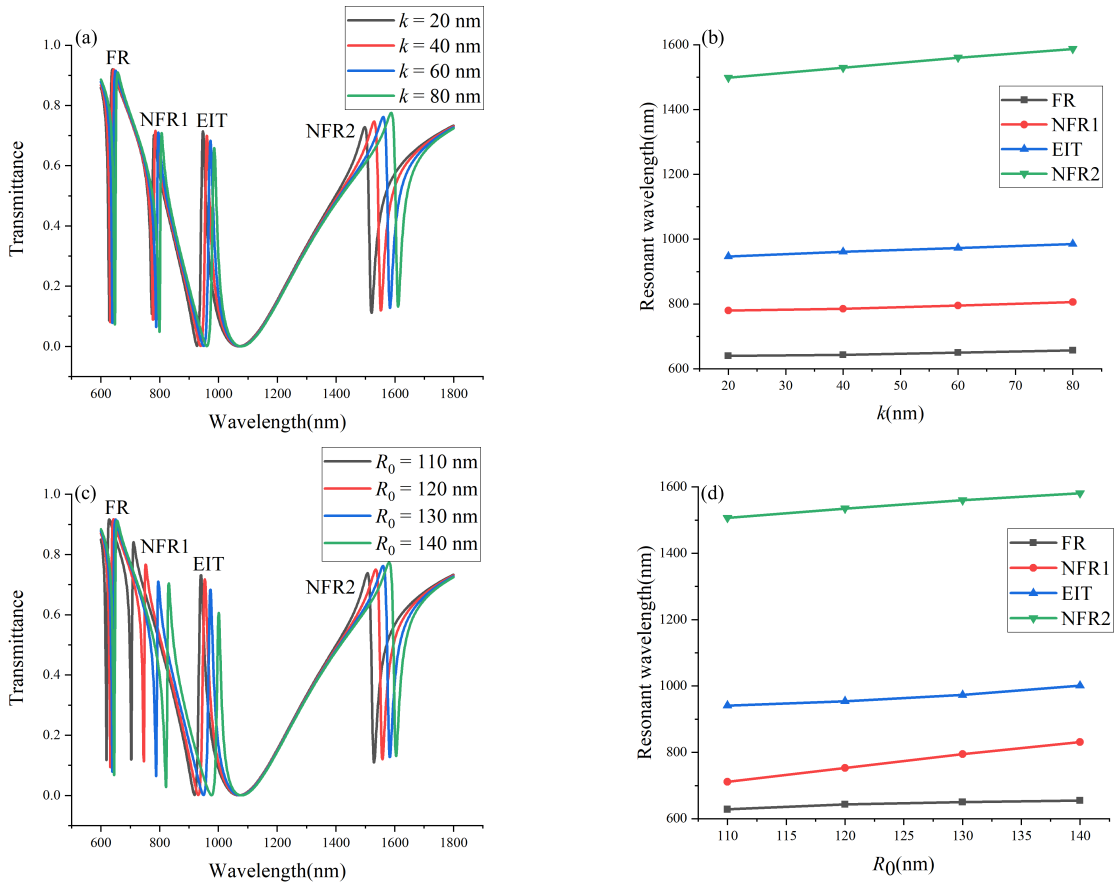

FIGURE 5. (a) The transmission spectra of the derived structure with changing from 20 nm to 80 nm. (b) The resonant wavelengths of FR, NFR, EIT and NFR2 with different k. (c) The transmission spectra of the derived structure with varying R_0 from 110nm to 140nm. (d) The resonant wavelengths of FR, NFR, EIT and NFR2 with different R_0.

V. QUADRUPLE FANO RESONANCES AND TRIPLE EIT-LIKE RESPONSES BY INTRODUCING ANOTHER RING CAVITY

To further improve the sensing performance of the system in section III.A and provide more sensing check-points and even to design multi-spectrum sensor, another ring cavity is added under the stub MIM waveguide with the distance g of 10 nm, as shown in figure 6(a). The thickness of the lower ring cavity is also set as $w = 50$ nm, and the radius $R_1 = 250$ nm. The transmission spectra of the system in Section III.A and III.B are shown in figure 6(b). It should be observed that the resonant wavelengths of FR, NFR1, EIT, and NFR2 basically remain unchanged. Besides, two new Fano resonance line-shapes arise, marked as NFR3 and NEIT. In comparison with figure 6(b), the wavelengths of rapid phase shift change in figure 6(c) are coincident with the resonant wavelengths of FR, NFR3, NFR1, EIT, NEIT, and NFR2, respectively. To further explore the origin of quadruple Fano resonances and double EIT-like effects, the field intensity ($|H_z|^2$) distribution at the peak of FR ($\lambda = 648$ nm), NFR3 ($\lambda = 703$ nm), NFR1 ($\lambda = 796$ nm), EIT ($\lambda = 971$ nm), NEIT ($\lambda = 1009$ nm), NFR2 ($\lambda = 1561$ nm) are displayed in figure 6 (d)-(i), respectively. The $|H_z|^2$ distributions at FR, NFR1, EIT, and NFR2 are nearly identical to those in figure 4 (d)-(g), which indicates that FR is still largely influenced by ring mode, NFR1 is still mainly caused by inner ring mode, EIT and NFR2 are mainly induced by ring-inner ring mode based on the discussion in section III.A. Nevertheless, compared with figure 4(d) and (f), a small portion of the energy in figure 6 (d) and (g) is restricted in the lower ring, resulting in a lower transmittance of the system in section III.B than that in section III.A. In figure 6 (e) and (h), the SPPs are confined in the lower ring cavity at $\lambda = 648$ nm (NFR3) and $\lambda = 703$ nm (NEIT), exciting a new high-order mode (dark mode) termed as lower ring mode. The NFR3 and NEIT originate from the interference between the lower ring mode and the low-order resonant mode (bright mode) from the stub.

VI. POTENTIAL APPLICATIONS OF THE PROPOSED MULTIPLE FANO AND EIT-LIKE RESONANCES STRUCTURES

A. SENSING POTENTIAL OF THE STRUCTURES

The sensing performance of our structures above is illustrated with its response for different refractive indices of the white etches in figure 4(a) and 6(a). The structural parameters are those used in figure 4(a) and 6(a), and the refractive index n varies from 1.00 to 1.03 at interval of 0.01.

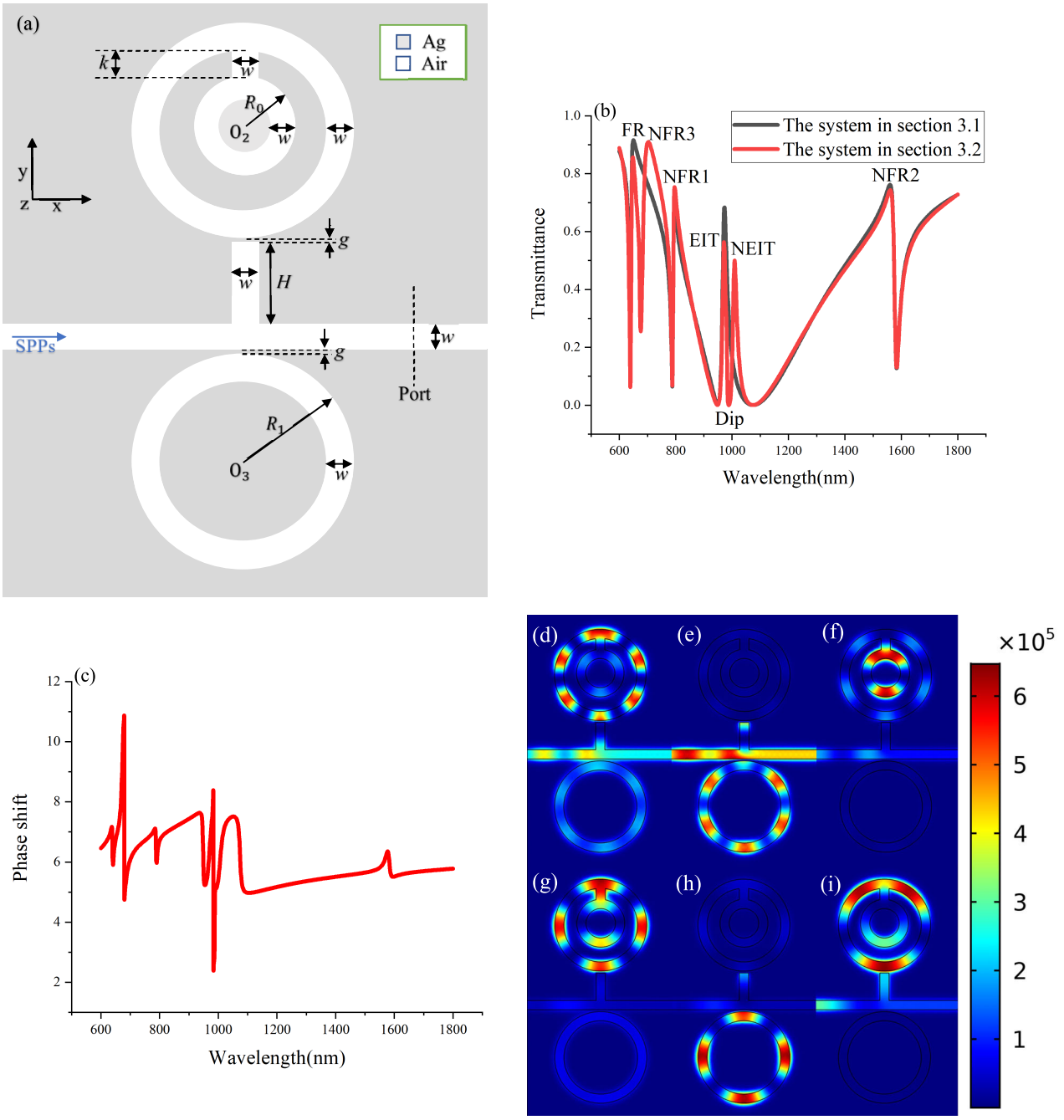

FIGURE 6. (a) Schematic diagram of the derived structure in section III.B (b) The black and red lines denote the transmission spectrum of the proposed structure in section III.A and the derived structure in section III.B (c) The phase shift spectrum of the derived structure. (d)-(j) The field intensity ($|H_z|^2$) distribution at the peak of FR(λ = 648 nm), NFR3(λ = 703 nm), NFR1(λ = 796 nm), EIT(λ = 971 nm), NEIT(λ = 1009 nm), NFR2 (λ = 1561 nm).

The sensing performance of the derived structure in section III.A is displayed in figure 7(a), which shows that these triple Fano resonances and single EIT-like response have a redshift when n increases from 1.00 to 1.03. The sensitivity(S) of the refractive index sensor can be defined as the shift in the resonance wavelength per unit change of the refractive index, as defined as $S = d\lambda/dn(nm/RIU)$ [6]. Thus, the S are 600 nm/RIU, 800 nm/RIU, 1000 nm/RIU, and 1600 nm/RIU at FR, NFR1, EIT, and NFR2, respectively, which can be obtained from figure 7(b).

The FOM is another crucial and more illustrative parameter to evaluate the sensing performance of the system, expressed as $FOM = \Delta T/T\Delta n$ [20], where T is the transmittance of the system and $\Delta T/\Delta n$ denotes the transmittance variation at the constant wavelength induced by the alteration of n. As can be seen from figure 7(c), the FOMs are calculated for the refractive indexes 1.01, 1.02, and 1.03 as $FOM = (T_{n=1.01/1.02/1.03} - T_{n=1})/(T_{n=1}\Delta n)$, among which the maximum can reach 2685 at 949 nm, which is larger than that in the previous report about refractive index sensors [40], [50], [53].

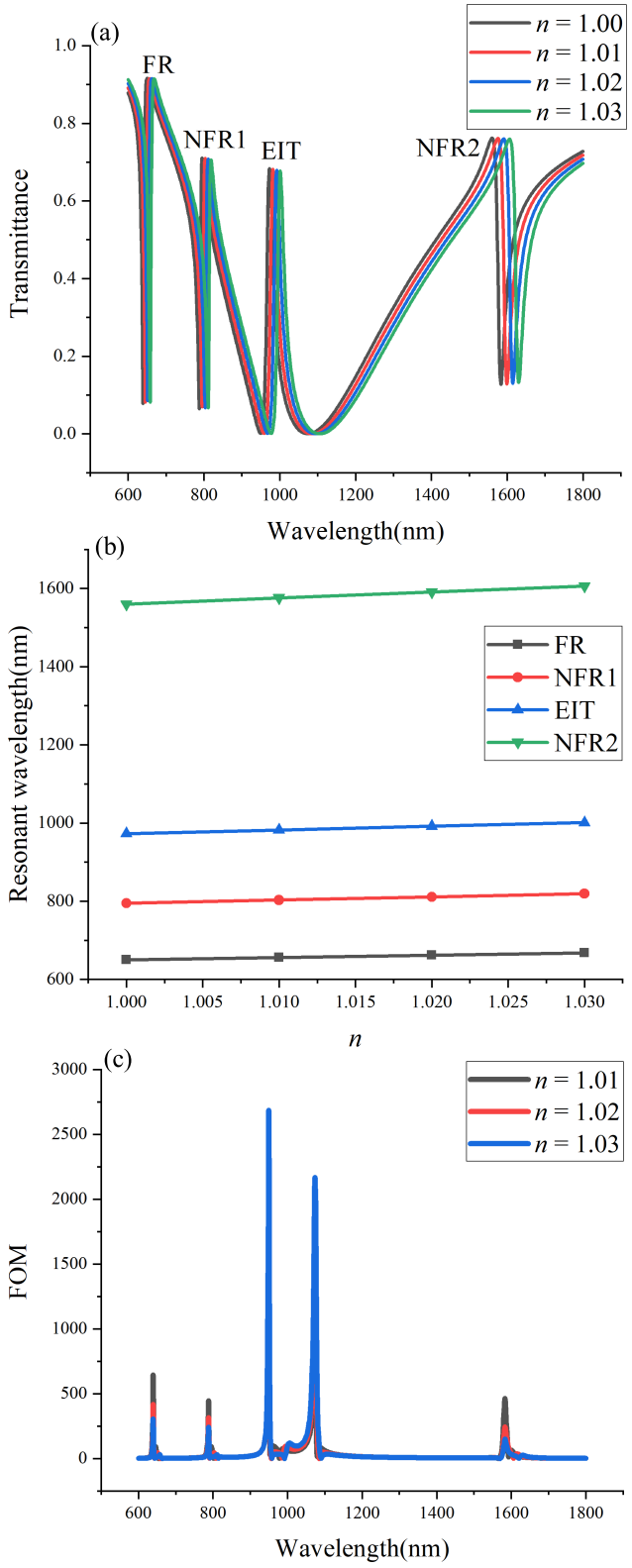

FIGURE 7. (a) The transmission spectra of the derived structure in section III.A with variable n from 1 to 1.03. (b) The resonant wavelengths of FR, NFR1, EIT and NFR2 with variable n. (c) Calculated FOM for different n.

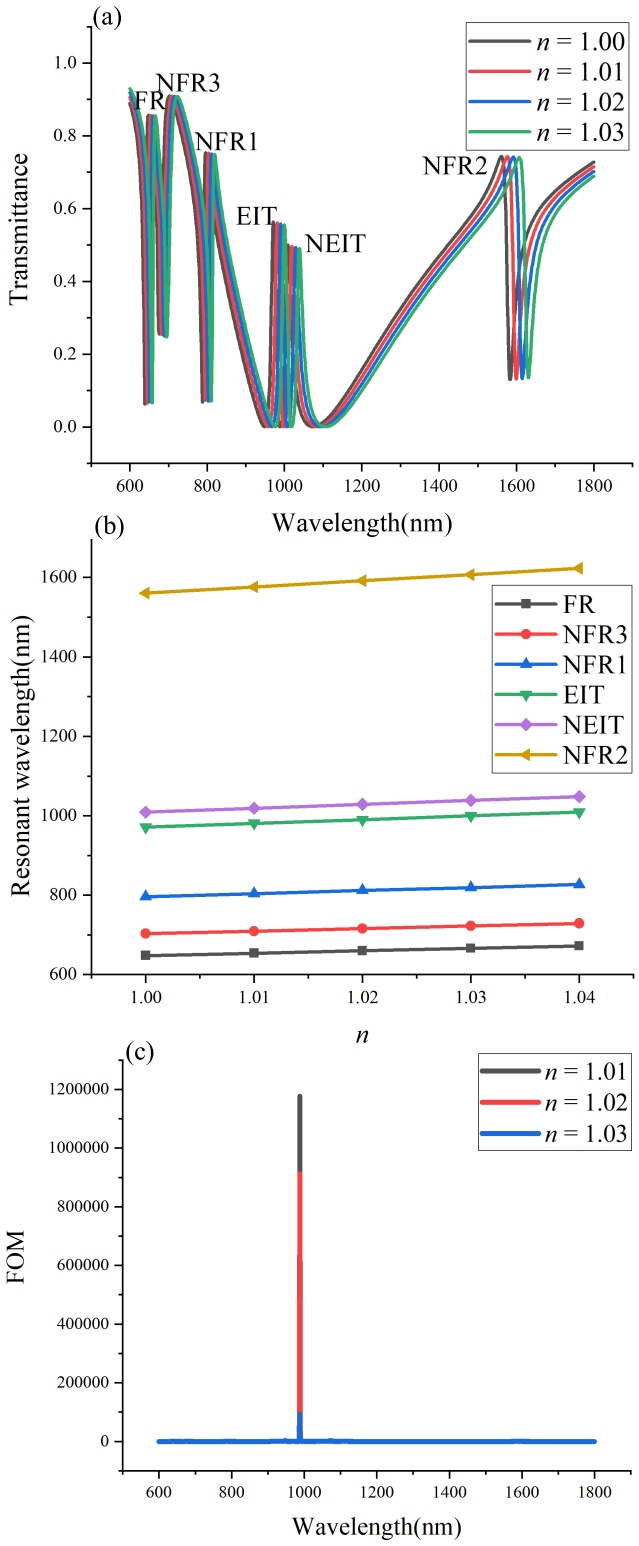

FIGURE 8. (a) The transmission spectra of the derived structure in section III.B with variable n from 1 to 1.03. (b) The resonant wavelengths of FR, NFR3, NFR1, EIT, NEIT and NFR2 with variable n. (c) Calculated FOM for different n.

Similarly, we further explore the sensing potential of the derived system in section III.B, which is displayed in figure 8(a), (b) and (c). Herein, the proposed structure still has great sensitivity, about 600 nm/RIU, 700 nm/RIU, 800 nm/RIU, 1000 nm/RIU, 1000 nm/RIU, 1600 nm/RIU at FR, NFR3, NFR1, EIT, NEIT, and NFR2, respectively.

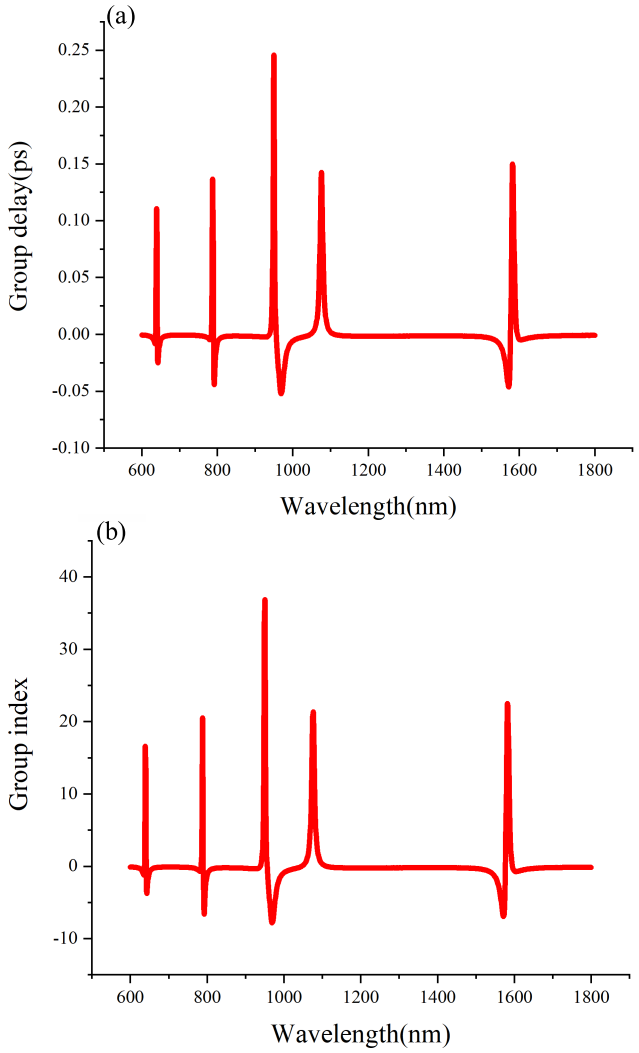

FIGURE 9. (a) The delay time of the derived structure in section III.A. (b) The group index of the derived structure in section III.A.

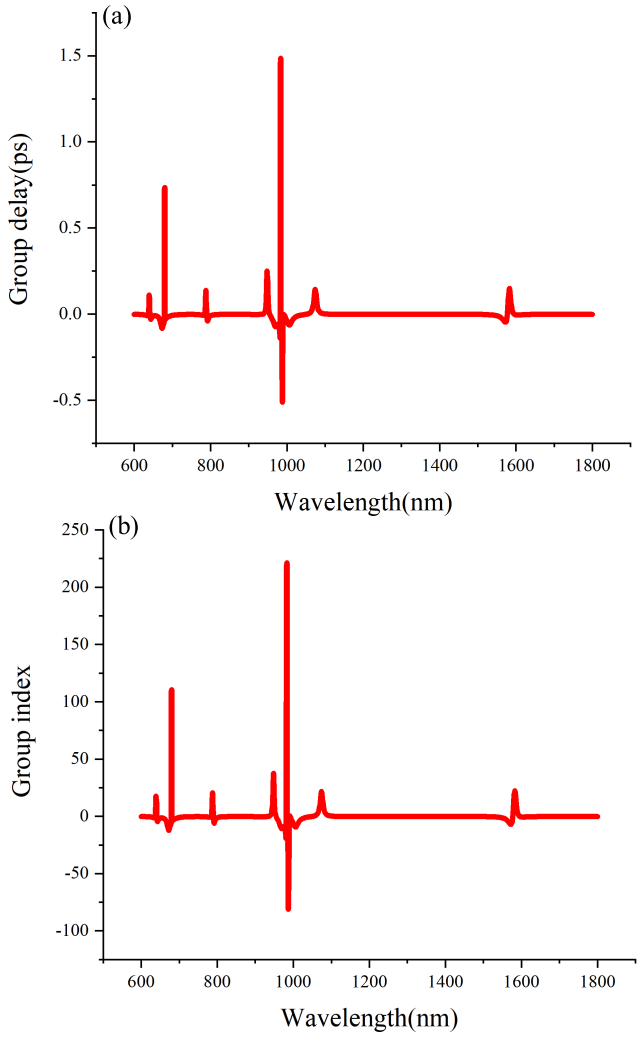

FIGURE 10. (a) The delay time of the derived structure in section III.B. (b) The group index of the derived structure in section III.B.

As shown in figure 8(c), though these FOM lines are different in the maximal values, it is noteworthy that the maximum FOM can reach the order of 10^6 in the case of EIT, which is remarkably higher than the vast majority of proposed refractive index nanosensors [6], [18]–[21], [40]–[45], [53], [55], [63], [65]–[67].

B. SLOW LIGHT EFFECTS OF THE MULTIPLE FANO AND EIT-LIKE RESONANCES

Analogous to conventional EIT in atomic systems, the proposed EIT-like resonator above can also induce rapid phase changing and support slow group velocities, which is needed by the slow light applications. The slow light effects can be assessed by the group delay time τ_g(ps) and the group index n_g, which are expressed as [54], [56]

$$\tau_g = \frac{d\psi(\omega)}{d\omega} = -\frac{\lambda^2}{2\pi c}\frac{d\psi(\lambda)}{d\lambda} \tag{13}$$

$$n_g = \frac{c}{v_g} = \frac{c}{D}\tau_g = -\frac{\lambda^2}{2\pi D}\frac{d\psi(\lambda)}{d\lambda} \tag{14}$$

where ψ (λ) and c are transmission phase shift and the speed of light in vacuum, respectively, v_g is the group velocity of the EIT-like structure and $D = 2$ um is the length from the incident light to the output port. According to equations (13), (14) and figure 4(c), the $\tau_g(ps)$ and n_g are numerically calculated, which are shown in figure 9 (a) and (b). It can be seen that the maximum delay time and group index are about 0.25 ps and 37 at around NEIT, which are around five times of those of the Fano system [57].

In the same way, figure 10 (a) and (b) represent the $\tau_g(ps)$ and n_g. Obviously, there are large group delays and indexes around the Fano and EIT-like resonances, among which the maximum delay time and group index are about 1.49 ps and 221 at around EIT, which are around six times of those of the system presented in section III.A.

C. SWITCHING APPLICATIONS OF THE SYSTEM

Optical switch is essential for the next generation of highly integrated optical circuits [54], [58]. The steep Fano and EIT-like line shapes proposed in this literature are ideal for

TABLE 1. Comparison of the proposed structure and the latest relevant structures.

Reference	Type	S	FOM	τ_g	n_g	EXT
[6]	4	500/850/950/1300	Max 4.038×10^3	N/A	N/A	N/A
[7]	1	1280	N/A	N/A	N/A	30dB
[18]	4	680/820/840/1100	Max 3.2×10^5	N/A	N/A	N/A
[19]	1	1400	2.3×10^4	N/A	N/A	N/A
[20]	3 4	800/1300/2000 650/900/1350/2000	Max 4.05×10^4 Max 4452	0.61ps 1.17ps	N/A	N/A
[21]	3	760/1320/1640	Max 3.7×10^4	N/A	N/A	N/A
[23]	1	1057	N/A	N/A	N/A	N/A
[40]	1	733	695	N/A	N/A	N/A
[41]	4	650/750/1100/950	Max 2.73×10^4	N/A	N/A	N/A
[42]	4	800/1000/1600/1900	Max 3.8×10^4	N/A	N/A	N/A
[43]	2	850/1120	Max 1.7×10^5	N/A	N/A	N/A
[44]	4	416/520/866/986	Max 3.2×10^5	N/A	N/A	N/A
[45]	2	1350/800	Max 3.51×10^4	N/A	N/A	91dB
[53]	2	1040/980	198.9/197.6	N/A	N/A	N/A
[54]	1	N/A	N/A	N/A	26	N/A
[55]	1	1277	2.2×10^4	N/A	180	N/A
[56]	1	N/A	N/A	N/A	51	N/A
[57]	1	800	N/A	0.053ps	N/A	N/A
[59]	N/A	N/A	N/A	N/A	N/A	16.6dB,10.37dB
[60]	N/A	N/A	N/A	N/A	N/A	32.1dB
[64]	1	903	Max 4.6×10^5	N/A	N/A	N/A
[65]	1	1260	Max 2.3×10^4	N/A	N/A	N/A
[66]	1	718	Max 4354	N/A	N/A	N/A
[67]	3 to 7	Max 1382	Max 48.6dB ($10^{4.86}$)	0.14ps	N/A	N/A
This work	6	600/700/800/1000/1000/1600	Max 1.2×10^6	1.49ps	221	43dB

devising all-optical switches. As shown in figure 6(b), the transmittance of the proposed structure can sharply drop from EIT peak (''on state'') to EIT dip (''off state'') with wavelength shifts about 17 nm, and thus this characteristic can be used for designing an all-optical switch. The on/off extinction ratio is a key indicator to evaluate the performance of the optical switch, which is expressed as [59]

$$EXT = 10\lg\frac{T_{max}}{T_{min}}\ (\mathrm{dB}) \tag{15}$$

where T_{max} and T_{min} represent the transmission of the peak (''on state'') and dip (''off state''), separately. According to the formula above, the extinction ratio at EIT is about 43 dB, which is great higher than the previous researches [7], [59], [60]. This work lays the groundwork for the design of high-performance optical switches with fast response combined with Kerr materials in the future. [63], [68]

Finally, in order to clearly illustrate the advantages of the proposed structure in various applications, the table 1 is made, which compares the performance parameters of our structure with those of other similar structures and systems which can produce multiple Fano or EIT-like resonances published in recent years. In this table, type represents the number of Fano or EIT-like profiles of a system. From the table we can draw the conclusion that our structure has relatively good sensitivity and it is superior to other structures in both the maximal FOM and the number of Fano or EIT-like resonances [6], [18]–[21], [40]–[45], [53], [55], [64]–[67]. Besides, the slow light effects of our system outperform other researches in the reference [20], [54]–[57], which shows great promises for highly integrated slow light applications. And it is worth mentioning that the extinction ratio of the proposed system is higher than that of most other proposed structures in the reference [7], [59], [60]. All in all, the proposed structure can play a significant role in highly integrated plasmonic devices including refractive index sensors, slow light devices, optical switches.

VII. CONCLUSION

In summary, Fano resonance and EIT-like effect in the basic proposed structure are numerically calculated. Based on this, an inner ring is introduced to create a new coupled plasmonic structure, which provides triple Fano resonances and single EIT-like profile and yields an ideal sensitivity of 1600 nm/RIU but the maximal FOM value of 2685 is not high enough. Besides, its maximum group delay time and group index are about 0.25 ps and 37. Such properties are greatly improved by adding another ring cavity under the stub MIM waveguide to create a new coupled plasmonic structure as well, providing quadruple Fano resonances and double EIT-like effects and yielding a great sensitivity of 1600 nm/RIU and the ultra-high maximal FOM

value of 1.2×10^6, which is better than the vast majority of researches up to the present. Moreover, a maximum group delay time and group index about 1.49 ps and 221 at around EIT can be realized, which is quite promising for on-chip slow light applications. Finally, an all-optical switch is also studied based on the EIT-like resonance with an on/off contrast ratio about 43 dB. It is believed that the proposed structures can support substantial excellent applications such as bio-chemical nanosensors, slow light and nonlinear devices, optical switches and filters in highly integrated plasmonic devices.

REFERENCES

[1] Z. Han and S. I. Bozhevolnyi, "Radiation guiding with surface plasmon polaritons," *Rep. Prog. Phys.*, vol. 76, no. 1, Jan. 2013, Art. no. 016402.
[2] A. V. Zayats, I. I. Smolyaninov, and A. A. Maradudin, "Nano-optics of surface plasmon polaritons," *Phys. Rep.*, vol. 408, nos. 3–4, pp. 131–314, Mar. 2005.
[3] W. L. Barnes, A. Dereux, and T. W. Ebbesen, "Surface plasmon subwavelength optics," *Nature*, vol. 424, no. 6950, pp. 824–830, Aug. 2003.
[4] P. Berini, "Plasmon-polariton waves guided by a metal film of finite width bounded by different dielectrics," *Opt. Express*, vol. 7, no. 10, pp. 329–335, Dec. 2000.
[5] H. Lu, X. Liu, L. Wang, Y. Gong, and D. Mao, "Ultrafast all-optical switching in nanoplasmonic waveguide with Kerr nonlinear resonator," *Opt. Express*, vol. 19, no. 4, p. 2910, Feb. 2011.
[6] T. Zhao and S. Yu, "Ultra-high sensitivity nanosensor based on multiple Fano resonance in the MIM coupled plasmonic resonator," *Plasmonics*, vol. 13, no. 4, pp. 1115–1120, Aug. 2018.
[7] Z. Chen, X. Song, G. Duan, L. Wang, and L. Yu, "Multiple Fano resonances control in MIM side-coupled cavities systems," *IEEE Photon. J.*, vol. 7, no. 3, pp. 1–10, Jun. 2015.
[8] X. Piao, S. Yu, S. Koo, K. Lee, and N. Park, "Fano-type spectral asymmetry and its control for plasmonic metal-insulator-metal stub structures," *Opt. Express*, vol. 19, no. 11, pp. 10907–10912, May 2011.
[9] J. A. Fan, C. Wu, K. Bao, J. Bao, R. Bardhan, N. J. Halas, V. N. Manoharan, P. Nordlander, G. Shvets, and F. Capasso, "Self-assembled plasmonic nanoparticle clusters," *Science*, vol. 328, no. 5982, pp. 1135–1138, May 2010.
[10] M. Hentschel, M. Saliba, R. Vogelgesang, H. Giessen, A. P. Alivisatos, and N. Liu, "Transition from isolated to collective modes in plasmonic oligomers," *Nano Lett.*, vol. 10, no. 7, pp. 2721–2726, Jul. 2010.
[11] Y. Zhu, X. Hu, Y. Huang, H. Yang, and Q. Gong, "Fast and low-power all-optical tunable Fano resonance in plasmonic microstructures," *Adv. Opt. Mater.*, vol. 1, no. 1, pp. 61–67, Jan. 2013.
[12] K. Wen, L. Yan, W. Pan, B. Luo, Z. Guo, Y. Guo, and X. Luo, "Electromagnetically induced transparency-like transmission in a compact side-coupled T-shaped resonator," *J. Lightw. Technol.*, vol. 32, no. 9, pp. 1701–1707, May 1, 2014.
[13] R. Zia, J. A. Schuller, A. Chandran, and M. L. Brongersma, "Plasmonics: The next chip-scale technology," *Mater. Today*, vol. 9, nos. 7–8, pp. 20–27, Jul. 2006.
[14] Y. Fang and M. Sun, "Nanoplasmonic waveguides: Towards applications in integrated nanophotonic circuits," *Light Sci. Appl.*, vol. 4, no. 6, p. e294, Jun. 2015.
[15] T. Xu, Y. K. Wu, X. Luo, and L. J. Guo, "Plasmonic nanoresonators for high-resolution colour filtering and spectral imaging," *Nature Commun.*, vol. 1, no. 5, pp. 118–124, Aug. 2010.
[16] G. Veronis and S. Fan, "Bends and splitters in metal-dielectric-metal subwavelength plasmonic waveguides," *Appl. Phys. Lett.*, vol. 87, no. 13, Sep. 2005, Art. no. 131102.
[17] E. N. Economou, "Surface plasmons in thin films," *Phys. Rev.*, vol. 182, no. 2, pp. 539–554, Jul. 2002.
[18] Z. Chen and L. Yu, "Multiple Fano resonances based on different waveguide modes in a symmetry breaking plasmonic system," *IEEE Photon. J.*, vol. 6, no. 6, pp. 1–8, Dec. 2014.
[19] X. Ren, K. Ren, and Y. Cai, "Tunable compact nanosensor based on Fano resonance in a plasmonic waveguide system," *Appl. Opt.*, vol. 56, no. 31, p. H1, Nov. 2017.
[20] S. Yu, T. Zhao, J. Yu, and D. Pan, "Tuning multiple Fano resonances for on-chip sensors in a plasmonic system," *Sensors*, vol. 19, no. 7, p. 1559, Apr. 2019.
[21] Z. Chen, X. Cao, X. Song, L. Wang, and L. Yu, "Side-coupled cavity-induced Fano resonance and its application in nanosensor," *Plasmonics*, vol. 11, no. 1, pp. 307–313, Feb. 2016.
[22] Q. Lu, Z. Wang, Q. Huang, W. Jiang, Z. Wu, Y. Wang, and J. Xia, "Plasmon-induced transparency and high-performance slow light in a plasmonic single-mode and two-mode resonators coupled system," *J. Lightw. Technol.*, vol. 35, no. 9, pp. 1710–1717, May 1, 2017.
[23] Z. D. Zhang, R. B. Wang, Z. Y. Zhang, J. Tang, W. D. Zhang, C. Y. Xue, and S. B. Yan, "Electromagnetically induced transparency and refractive index sensing for a plasmonic waveguide with a stub coupled ring resonator," *Plasmonics*, vol. 12, no. 4, pp. 1007–1013, Aug. 2017.
[24] Y. Cui and C. Zeng, "All-optical EIT-like phenomenon in plasmonic stub waveguide with ring resonator," *Opt. Commun.*, vol. 297, pp. 190–193, Jun. 2013.
[25] T. Nurmohammadi, K. Abbasian, and R. Yadipour, "Ultra-fast all-optical plasmonic switching in near infra-red spectrum using a Kerr nonlinear ring resonator," *Opt. Commun.*, vol. 410, pp. 142–147, Mar. 2018.
[26] G. Zhan, R. Liang, H. Liang, J. Luo, and R. Zhao, "Asymmetric band-pass plasmonic nanodisk filter with mode inhibition and spectrally splitting capabilities," *Opt. Express*, vol. 22, no. 8, p. 9912, Apr. 2014.
[27] Z. Chen, M. Chen, J. Li, L. Wang, R. Jiao, G. Duan, L. Yu, and J. Xiao, "Symmetry breaking induced mode splitting based on a plasmonic waveguide system," *J. Phys. D, Appl. Phys.*, vol. 49, no. 14, Apr. 2016, Art. no. 145109.
[28] F. Hu, H. Yi, and Z. Zhou, "Wavelength demultiplexing structure based on arrayed plasmonic slot cavities," *Opt. Lett.*, vol. 36, no. 8, p. 1500, Apr. 2011.
[29] M. DiChristina, B. S. Meyerson. *The Top 10 Emerging Technologies of 2018*. Accessed: Oct. 2018. [Online]. Available: https://www.scientificamerican.Com/article/the-top-10-emerging-technologies-of-2018/
[30] S. Zhan, H. Li, G. Cao, Z. He, B. Li, and H. Xu, "Theoretical analysis of plasmon-induced transparency in ring-resonators coupled channel drop filter systems," *Plasmonics*, vol. 9, no. 6, pp. 1431–1437, Dec. 2014.
[31] Z.-D. Zhang, H.-Y. Wang, and Z.-Y. Zhang, "Fano resonance in a gear-shaped nanocavity of the metal–insulator–metal waveguide," *Plasmonics*, vol. 8, no. 2, pp. 797–801, Jun. 2013.
[32] L. F. Niu, "Fano resonance in dual-disk ring plasmonic nanostructure," *Opt. Express*, vol. 19, no. 23, pp. 22974–22981, Nov. 2011.
[33] A. E. Miroshnichenko, S. Flach, and Y. S. Kivshar, "Fano resonances in nanoscale structures," *Rev. Mod. Phys.*, vol. 82, no. 3, pp. 2257–2298, Aug. 2010.
[34] B. Luk'yanchuk, N. I. Zheludev, S. A. Maier, N. J. Halas, P. Nordlander, H. Giessen, and C. T. Chong, "The Fano resonance in plasmonic nanostructures and metamaterials," *Nature Mater.*, vol. 9, no. 9, pp. 707–715, Sep. 2010.
[35] B. Peng, S. K. Özdemir, W. Chen, F. Nori, and L. Yang, "What is and what is not electromagnetically induced transparency in whispering-gallery microcavities," *Nature Commun.*, vol. 5, no. 1, pp. 509–5082, Dec. 2014.
[36] K.-J. Boller, A. Imamoğlu, and S. E. Harris, "Observation of electromagnetically induced transparency," *Phys. Rev. Lett.*, vol. 66, no. 20, pp. 2593–2596, Jul. 2002.
[37] D. D. Smith, "Coupled-resonator-induced transparency," *Phys. Rev. A, Gen. Phys.*, vol. 69, no. 6, pp. 666–670, Jun. 2004.
[38] L.-Y. He, T.-J. Wang, Y.-P. Gao, C. Cao, and C. Wang, "Discerning electromagnetically induced transparency from Autler-Townes splitting in plasmonic waveguide and coupled resonators system," *Opt. Express*, vol. 23, no. 18, p. 23817, Sep. 2015.
[39] M. Hu, F. Wang, R. Liang, S. Zhou, and L. Xiao, "Plasmonic-induced transparency based on plasmonic asymmetric dual side-coupled cavities," *Phys. Lett. A*, vol. 379, no. 6, pp. 581–584, Mar. 2015.
[40] B. Ni, X. Y. Chen, D. Y. Xiong, H. Liu, G. H. Hua, J. H. Chang, J. H. Zhang, and H. Zhou, "Infrared plasmonic refractive index-sensitive nanosensor based on electromagnetically induced transparency of waveguide resonator systems," *Opt. Quantum Electron.*, vol. 47, no. 6, pp. 1339–1346, Jun. 2015.
[41] C. Li, S. Li, Y. Wang, R. Jiao, L. Wang, and L. Yu, "Multiple Fano resonances based on plasmonic resonator system with end-coupled cavities for high-performance nanosensor," *IEEE Photon. J.*, vol. 9, no. 6, pp. 1–9, Dec. 2017.

[42] Y. Zhang, S. Li, Z. Chen, P. Jiang, R. Jiao, Y. Zhang, L. Wang, and L. Yu, "Ultra-high sensitivity plasmonic nanosensor based on multiple Fano resonance in the MDM side-coupled cavities," *Plasmonics*, vol. 12, no. 4, pp. 1099–1105, Aug. 2017.
[43] J. Yang, X. Song, Z. Chen, L. Cui, S. Yang, and L. Yu, "Tunable multi-Fano resonances in MDM-based side-coupled resonator system and its application in nanosensor," *Plasmonics*, vol. 12, no. 6, pp. 1665–1672, Dec. 2017.
[44] N. Jankovic and N. Cselyuszka, "Multiple Fano-like MIM plasmonic structure based on triangular resonator for refractive index sensing," *Sensors*, vol. 18, no. 1, p. 287, Jan. 2018.
[45] Y. Wang, S. Li, Y. Zhang, and L. Yu, "Ultrasharp Fano resonances based on the circular cavity optimized by a metallic nanodisk," *IEEE Photon. J.*, vol. 8, no. 6, pp. 1–8, Dec. 2016.
[46] X.-S. Lin and X.-G. Huang, "Tooth-shaped plasmonic waveguide filters with nanometeric sizes," *Opt. Lett.*, vol. 33, no. 23, p. 2874, Dec. 2008.
[47] Y. Gong, X. Liu, and L. Wang, "High-channel-count plasmonic filter with the metal-insulator-metal Fibonacci-sequence gratings," *Opt. Lett*, vol. 35, no. 3, p. 285, Jan. 2010.
[48] F. Hu, H. Yi, and Z. Zhou, "Band-pass plasmonic slot filter with band selection and spectrally splitting capabilities," *Opt. Express*, vol. 19, no. 6, pp. 4848–4855, Mar. 2011.
[49] C. Zeng, Y. Cui, and X. Liu, "Tunable multiple phase-coupled plasmon-induced transparencies in graphene metamaterials," *Opt. Express*, vol. 23, no. 1, pp. 545–551, Jan. 2015.
[50] H. Lu, X. Liu, D. Mao, and G. Wang, "Plasmonic nanosensor based on Fano resonance in waveguide-coupled resonators," *Opt. Lett.*, vol. 37, no. 18, p. 3780, Sep. 2012.
[51] H. Haus and W. P. Huang, "Coupled-mode theory," *Proc. IEEE*, vol. 79, no. 10, pp. 1505–1518, Oct. 1991.
[52] S. Li, Y. Wang, R. Jiao, L. Wang, G. Duan, and L. Yu, "Fano resonances based on multimode and degenerate mode interference in plasmonic resonator system," *Opt. Express*, vol. 25, no. 4, pp. 3525–3533, Feb. 2017.
[53] H. Fu, S. Li, Y. Wang, G. Song, P. Zhang, L. Wang, and L. Yu, "Independently tunable ultrasharp double Fano resonances in coupled plasmonic resonator system," *IEEE Photon. J.*, vol. 10, no. 1, pp. 1–9, Feb. 2018.
[54] Z. Han and S. I. Bozhevolnyi, "Plasmon-induced transparency with detuned ultracompact Fabry-Perot resonators in integrated plasmonic devices," *Opt. Express*, vol. 19, no. 4, pp. 3251–3257, Feb. 2011.
[55] Y. Binfeng, Z. Ruohu, H. Guohua, and C. Yiping, "Ultra sharp Fano resonances induced by coupling between plasmonic stub and circular cavity resonators," *Plasmonics*, vol. 11, no. 4, pp. 1157–1162, Aug. 2016.
[56] S. Zhan, H. Li, G. Cao, Z. He, B. Li, and H. Yang, "Slow light based on plasmon-induced transparency in dual-ring resonator-coupled MDM waveguide system," *J. Phys. D, Appl. Phys.*, vol. 47, no. 20, May 2014, Art. no. 205101.
[57] F. Chen, "Nanosensing and slow light application based on Fano resonance in waveguide coupled equilateral triangle resonator system," *Optik*, vol. 171, pp. 58–64, Oct. 2018.
[58] K. Nozaki, A. Shinya, S. Matsuo, T. Sato, E. Kuramochi, and M. Notomi, "Ultralow-energy and high-contrast all-optical switch involving Fano resonance based on coupled photonic crystal nanocavities," *Opt. Express*, vol. 21, no. 10, p. 11877, May 2013.
[59] F. Chen and D. Yao, "Tunable multiple all-optical switch based on multi-nanoresonator-coupled waveguide systems containing Kerr material," *Opt. Commun.*, vol. 312, pp. 143–147, Feb. 2014.
[60] H. Liu, G. Ren, Y. Gao, B. Zhu, H. Li, B. Wu, and S. Jian, "Ultrafast and low-power all-optical switch based on asymmetry electromagnetically induced transparency in MIM waveguide containing Kerr material," *Opt. Commun.*, vol. 353, pp. 189–194, Oct. 2015.
[61] B. Yun, G. Hu, C. Jiawei, and Y. Cui, "Plasmon induced transparency in metal–insulator–metal waveguide by a stub coupled with F-P resonator," *Mater. Res. Express*, vol. 1, no. 3, Jul. 2014, Art. no. 036201.
[62] V. A. Fedotov, M. Rose, S. L. Prosvirnin, N. Papasimakis, and N. I. Zheludev, "Sharp trapped-mode resonances in planar metamaterials with a broken structural symmetry," *Phys. Rev. Lett.*, vol. 99, no. 14, p. 147401, Oct. 2007.
[63] S. Paul and M. Ray, "Simultaneous switching at multiple wavelengths using plasmon induced transparency and Fano resonance," *IEEE Photon. Technol. Lett.*, vol. 29, no. 9, pp. 739–742, May 1, 2017.
[64] K. Wen, Y. Hu, L. Chen, J. Zhou, L. Lei, and Z. Guo, "Fano resonance with ultra-high figure of merits based on plasmonic metal-insulator-metal waveguide," *Plasmonics*, vol. 10, no. 1, pp. 27–32, Feb. 2015.
[65] Z. Chen, L. Yu, L. Wang, G. Duan, Y. Zhao, and J. Xiao, "A refractive index nanosensor based on Fano resonance in the plasmonic waveguide system," *IEEE Photon. Technol. Lett.*, vol. 27, no. 16, pp. 1695–1698, Aug. 15, 2015.
[66] X. Zhao, Z. Zhang, and S. Yan, "Tunable Fano resonance in asymmetric MIM waveguide structur," *Sensors*, vol. 17, no. 7, p. 1494, Jun. 2017.
[67] Z. Li, K. Wen, L. Chen, L. Lei, J. Zhou, D. Zhou, Y. Fang, and B. Wu, "Control of multiple Fano resonances based on a subwavelength MIM coupled cavities system," *IEEE Access*, vol. 7, pp. 59369–59375, 2019.
[68] J. Tao, Q. J. Wang, and X. G. Huang, "All-optical plasmonic switches based on coupled nano-disk cavity structures containing nonlinear material," *Plasmonics*, vol. 6, no. 4, pp. 753–759, Dec. 2011.

SHUO WANG was born in Zoucheng, Shandong, China, in 1995. He received the bachelor's degree from Liaocheng University, in 2017. He is currently pursuing the master's degree in communications optoelectronics with the Beijing University of Posts and Telecommunications.

His research interests include surface plasmon polaritons(SPPs), the fundamental research of optoelectronics and simulation and numerical calculation of highly integrated plasmonic devices, such as sensors, filters, and all-optical switches.

TONGGANG ZHAO was born in Langfang, Hebei, China. He received the bachelor's degree from the Beijing Institute of Technology, in 2000, and the Ph.D. degree in electromagnetic field and microwave technology from the Beijing University of Posts and Telecommunications, in 2005.

From 2008 to 2016, he was an Associate Professor with the School of Electronic Engineering, Beijing University of Posts and Telecommunications. Since 2016, he has been a Professor. He is the author of three books and more than 60 articles and holds three patents of inventions. His research interests include nano sensor, all-optical devices, photoelectric detection and sensing technology, and optical information exchange.

SHILIN YU received the B.S. degree in optical information science and technology from the Beijing University of Posts and Telecommunications, Beijing, China, in 2016, where he is currently pursuing the Ph.D. degree in electronic science and technology.

His research interests include plasmonics, the fundamental research of nanophotonics and applications of nanostructures.

WENYUAN MA received the B.E. degree in electronic information science and technology from the Beijing University of Posts and Telecommunications, Beijing, China, in 2019, where he is currently pursuing the M.E. degree in optical engineering.

His research interests include the development of sensor and filter using the surface plasmon polaritons (SPPs), and the design of all-optical switch based on Kerr effect and SPPs structure.